Phasor-based dehomogenisation for microchannel cooling topology optimisation

Hao Li, Peter Dørffler Ladegaard Jensen, Rebekka Vaarum Woldseth, Joe Alexandersen

▶ **To cite this version:**

Hao Li, Peter Dørffler Ladegaard Jensen, Rebekka Vaarum Woldseth, Joe Alexandersen. Phasor-based dehomogenisation for microchannel cooling topology optimisation. 2024. hal-04839124

HAL Id: hal-04839124
https://hal.science/hal-04839124v1

Preprint submitted on 15 Dec 2024

HAL is a multi-disciplinary open access archive for the deposit and dissemination of scientific research documents, whether they are published or not. The documents may come from teaching and research institutions in France or abroad, or from public or private research centers.

L'archive ouverte pluridisciplinaire **HAL**, est destinée au dépôt et à la diffusion de documents scientifiques de niveau recherche, publiés ou non, émanant des établissements d'enseignement et de recherche français ou étrangers, des laboratoires publics ou privés.

Phasor-Based Dehomogenisation for Microchannel Cooling Topology Optimisation

Hao Li
Institute of Mechanical and Electrical Engineering
University of Southern Denmark
Odense, Denmark
hli@sdu.dk

Peter Dørffler Ladegaard Jensen
Department of Mechanical Engineering
Technical University of Denmark
Lyngby, Denmark
pdlj@dtu.dk

Rebekka Vaarum Woldseth
Centre Inria
Université de Lorraine
Villers-lés-Nancy, France
rebekka-vaarum.woldseth@inria.fr

Joe Alexandersen
Institute of Mechanical and Electrical Engineering
University of Southern Denmark
Odense, Denmark
joal@sdu.dk

***Abstract*—Efficient thermal management is critical for high-power electronics, with microchannel cooling providing enhanced heat dissipation in compact designs. Conventional topology optimisation (TO) methods often fail to capture fine-scale features without relying on extremely fine meshes, leading to high computational costs. This study proposes a homogenisation-based TO framework integrated with an on-the-fly phasor-based dehomogenisation technique. The phasor-based method efficiently maps homogenised designs to fine-scale microchannel networks, maintaining continuous variations in channel properties and improving robustness while reducing computational expense compared to the conventional projection-based method. An idealised two-dimensional chip with heterogeneous heat generation is used to demonstrate the integrated design workflow. The homogenisation-based TO is performed on a coarse 50×50 mesh, with the phasor-based dehomogenisation reconstructing fine-scale microchannel networks on a 3213×3213 mesh. The results show that the framework achieves a three orders-of-magnitude reduction in computational cost compared to hypothetical brute-force full-scale optimisation and a 35.3% improvement in thermal performance over traditional pin-fin designs (the initial guess). Limitations of the current study, such as refining the homogenisation model and incorporating irregular meshes, point to promising directions for future investigations.**

***keywords*—microchannel cooling, dehomogenisation, phasor noise, topology optimisation, conjugate heat transfer.**

I. Introduction

Efficient thermal management is essential for maintaining performance in high-power electronics, such as GPUs and AI accelerators. Recent work demonstrated hotspot-aware microfluidic cooling using topology optimisation (TO), highlighting the importance of custom cooling designs for managing heterogeneous power distributions [1]. However, challenges are associated with simulating and optimising the flow distribution in microchannels. The intricate nature of the flow requires fine-detailed geometric representations, necessitating fine meshes, which increases the associated computational costs. Reducing computational cost while maintaining design fidelity remains a key challenge.

The homogenisation-based approach models partial densities as porous microstructures, enabling the design of microfluidic devices with fine-scale features that can be produced using additive manufacturing [2], [3]. Dehomogenisation denotes the process of mapping a homogenised multi-scale representation of infinitesimal microstructures to a finite single-scale design [4]. To achieve this, a least-squares projection-based approach for approximating a conformal mapping has previously been utilised [5]. However, as the problem size and complexity increases, this approach becomes computationally expensive and unstable. The emphasis on orientation conformity can also lead to variations in unit-cell sizes, resulting in disconnected structures [6]. This is problematic in microchannel cooling, where disrupted coolant flow reduces heat transfer and increases the risk of localised overheating.

This paper introduces an integrated design workflow that combines homogenisation-based topology optimisation (TO) with phasor-based dehomogenisation [7] to optimise microchannel cooling designs. The methodology employs a two-scale approach, deriving Darcy's law as the asymptotic limit of the Stokes equations in a periodic porous medium. A single-class microstructure is utilised, and numerical homogenisation is performed to construct an offline library of effective permeability and conductivity. This library is subsequently incorporated into the online TO process to optimise microstructure parameters and orientation fields on a coarse mesh grid. Phasor noise, generated using complex Gabor kernels, facilitates continuous variations in channel properties while preserving global periodicity, enabling the creation of connected microchannel networks with intricate branching patterns on a fine-scale mesh grid.

The presented study considers an idealised two-dimensional chip with the dimension of 1.0×1.0 units. The spatial distribution of heat flux across the chip surface (power map) is heterogeneous, as illustrated in Fig. 1. Specifically, the power

Marie Skłodowska-Curie Actions Postdoc Fellowship (no. 101106842).

map features four circular regions with higher heat generation rates compared to the rest of the surface. The chip is cooled by a coolant fluid flowing through a microchannel network embedded within a solid plate with relatively high thermal conductivity. The coolant fluid enters the domain through a centrally located inlet Γ_{in} on the left boundary with a parabolic velocity profile and exits through two outlets Γ_{out} positioned at the right edges of the top and bottom boundaries under a stress free condition.

The primary goal of this study is to optimise the microchannel network while integrating fine-scale features, thus avoiding the need for extremely fine meshes and maximum length scale constraints typically required in brute-force feature-rich topology optimisation methods [8], [9]. Consequently, the proposed design framework aims to achieve a significant reduction in computational costs by three orders-of-magnitude.

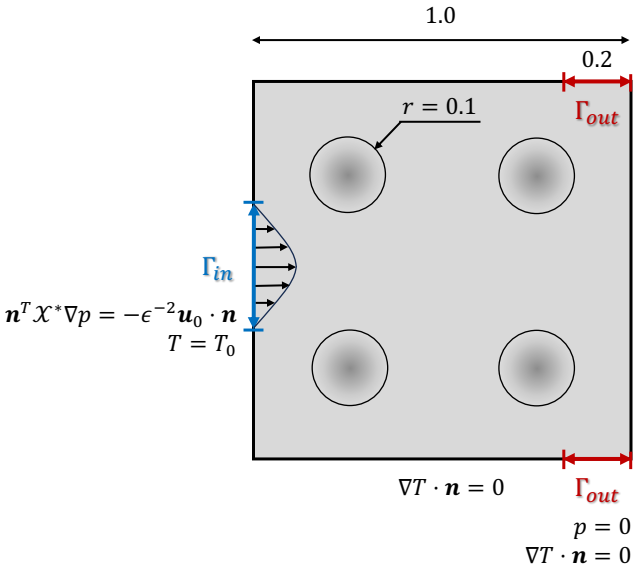

Fig. 1: Design schematic diagram. The coolant fluid enters the domain through the inlet Γ_{in} at the center of the left boundary with a parabolic profile and exits through the two outlets Γ_{out} at the right ends of the top and bottom boundaries. An inhomogeneous heat flux is applied on the surface, with higher heat generation in the four circular regions.

II. Methodology

In this section, we outline the methodology adopted in this work, starting with the homogenised problem for conjugate heat transfer in Section II-A. Next, we formulate the optimisation design problem in Section II-B and introduce the theoretical background of the phasor-based dehomogenisation method in Section II-C. Finally, the algorithm of the proposed design workflow is detailed in Section II-D.

A. Homomgenised problem

We consider a fixed, bounded domain $\Omega_\epsilon \subset \mathbb{R}^d$ $(d = 2)$, comprising periodic heterogeneous media composed of microscopic unit cells with characteristic length-scale ϵ. The domain Ω_ϵ is bounded by Dirichlet and Neumann boundaries, denoted by $\partial\Omega_\epsilon^D$ and $\partial\Omega_\epsilon^N$, respectively. Each unit cell is composed by two different isotropic material phases, i.e., fluid and solid, arranged in a square microstructure characterised by its width m_1, height m_2, and orientation angle θ, as shown in Fig. 2. These heterogeneous media can be approximated by a homogeneous medium with homogenised properties in the domain D, and the physical quantities of interest, such as fluid velocity $\boldsymbol{u}$, pressure p, and temperature T, are governed by the homogenisation equations.

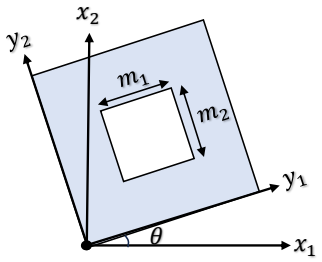

Fig. 2: Schematic diagram of the square microstructure with width m_1, height m_2, and orientation angle θ. The solid material phase is indicated as white, while the fluid material phase is indicated as light blue.

The considered creeping flow is governed by Stokes equations ($\text{Re} \ll 1$) in porous media. Since the late 1970s, studies [10]–[12] have shown that Darcy's law is derived as the asymptotic limit of the Stokes equations in periodic porous media as periodicity tends to be zero. The mathematical foundations and numerical validations are detailed in [13]–[15]. The nondimensional homogenised problem is described as

$$\begin{cases} \boldsymbol{u} = -\epsilon^2 \boldsymbol{\mathcal{X}}^* (m_1, m_2, \theta) \nabla p & \text{in } D, \\ \operatorname{div}(\boldsymbol{u}) = 0 & \text{in } D, \\ \boldsymbol{u} \cdot \boldsymbol{n} = \boldsymbol{u}_0 \cdot \boldsymbol{n} & \text{on } \Gamma_{\text{in}}, \\ p = 0 & \text{on } \Gamma_{\text{out}}, \end{cases} \tag{1}$$

where $\boldsymbol{\mathcal{X}}^* (m_1, m_2, \theta)$ denotes the global effective permeability matrix, which is scale-invariant and can be expressed as

$$\boldsymbol{\mathcal{X}}^* (m_1, m_2, \theta) = \boldsymbol{R}(\theta) \boldsymbol{\mathcal{X}}^H (m_1, m_2) \boldsymbol{R}(\theta)^T, \tag{2}$$

where $\boldsymbol{R}$ is the rotation matrix. The homogenised permeability $\boldsymbol{\mathcal{X}}_{ij}^H$ is computed by averaging the volumetric velocity for incompressible Stokes flow over the unit cell [16], [17].

The computed homogenised velocity $\boldsymbol{u}$ is then weakly coupled with the homogenised temperature T through the nondimensional homogenised convection-diffusion equation as

$$\begin{cases} \boldsymbol{u} \cdot \nabla T - \operatorname{div} \left(\boldsymbol{\mathcal{K}}^* (m_1, m_2, \theta) \nabla T \right) = Q(\boldsymbol{x}) & \text{in } D, \\ T = T_0 & \text{on } \Gamma_{\text{in}}, \\ \boldsymbol{\mathcal{K}}^* (m_1, m_2, \theta) \nabla T \cdot \boldsymbol{n} = 0 & \text{on } \partial D \backslash \Gamma_{\text{in}}, \end{cases} \tag{3}$$

where $\boldsymbol{\mathcal{K}}^* (m_1, m_2, \theta)$ is the global nondimensional diffusive tensor, which can be expressed as

$$\boldsymbol{\mathcal{K}}^* (m_1, m_2, \theta) = \boldsymbol{R}(\theta) \boldsymbol{\mathcal{K}}^H (m_1, m_2) \boldsymbol{R}(\theta)^T, \tag{4}$$

where $\boldsymbol{\mathcal{K}}_{ij}^H$ denotes the homogenised thermal conductivity

tensor which can be computed by averaging the volumetric heat flux over the unit cell. The volumetric heat source term $Q(\boldsymbol{x})$ is defined to reflect the heterogeneous heat generation across the domain as

$$Q(\boldsymbol{x}) = \begin{cases} 2.0 & \text{if } \left(x_1 - \frac{1}{4}\right)^2 + \left(x_2 - \frac{1}{4}\right)^2 \leq 0.1^2, \\ 2.0 & \text{if } \left(x_1 - \frac{1}{4}\right)^2 + \left(x_2 - \frac{3}{4}\right)^2 \leq 0.1^2, \\ 0.5 & \text{if } \left(x_1 - \frac{3}{4}\right)^2 + \left(x_2 - \frac{1}{4}\right)^2 \leq 0.1^2, \\ 0.5 & \text{if } \left(x_1 - \frac{3}{4}\right)^2 + \left(x_2 - \frac{3}{4}\right)^2 \leq 0.1^2, \\ 0.1 & \text{otherwise.} \end{cases} \tag{5}$$

B. Optimisation design problem

As has been discussed earlier, the goal is to optimise the microchannel network embedded within the solid plate to achieve efficient cooling of the chip. The design fields are therefore defined as the width m_1, height m_2, and orientation angle θ of the microstructures. The optimisation problem is formulated as a constrained minimisation problem, where the objective function $J(\Omega)$ is defined as the thermal compliance in the domain D, and the constraints are imposed to ensure the physical feasibility of the design fields. The optimisation problem is mathematically formulated as

$$\min_{m_1, m_2, \theta \in \mathcal{D}} J(\Omega) = \int_D Q(\boldsymbol{x})\, T \, \mathrm{d}\Omega, \tag{6a}$$

$$\text{s.t.} \begin{cases} \text{(1) and (3)}, \\ G_1 = \epsilon^2 \dfrac{1/\mathrm{DP}_0}{|\Gamma_{\text{in}}|} \displaystyle\int_{\Gamma_{\text{in}}} p \, \mathrm{d}\Gamma - C_{\mathrm{DP}} \leq 0, \\ G_2 = \dfrac{\int_D 1 - \hat{\tilde{m}}_1 \hat{\tilde{m}}_2 \, \mathrm{d}\Omega}{\int_D \mathrm{d}\Omega} - V_{\max} \leq 0, \\ 0 \leq m_1(\boldsymbol{x}), m_2(\boldsymbol{x}), \theta(\boldsymbol{x}) \leq 1 \quad \forall \boldsymbol{x} \in D, \end{cases} \tag{6b}$$

where G_1 and G_2 are the constraints on the pressure drop and volume, respectively. DP_0 denotes the pressure drop at the first iteration, C_{DP} represents the maximum allowed pressure drop fraction, and $V_{\max}$ is the maximum permitted volume fraction for the fluid phase. The sensitivity analysis is conducted using the discrete adjoint method, as detailed in [6]. The optimisation problem is solved using the Method of Moving Asymptotes (MMA) [18].

C. Phasor-based dehomogenisation

Phasor noise is a type of procedural noise function that can be used to efficiently generate perfectly contrasting oscillating wave-patterns with local control of periodicity and orientation [19]–[21]. By translating the multi-scale homogenised solution to a sparse set of signal-emitting phasor kernels, globally smooth rich texture content can be sampled at high resolutions, that locally adheres to specified orientations, thicknesses and length-scale. The phasor-based dehomogenisation approach takes advantage of these properties to perform efficient and scalable dehomogenisation of multi-scale minimum compliance optimised solutions [7]. This methodology has proven to provide improvements in robustness, unit-cell size control and efficiency compared to existing dehomogenisation methods in solid mechanics. The development of the `deHomTop808` educational code [22] integrating multi-scale topology optimisation and this dehomogenisation procedure to obtain on-the-fly dehomogenisation during the optimisation procedure proves the potential of this method, as well as making it accessible for future applications and research. The version of the phasor-based dehomogenisation approach utilised in this study is based on this publicly available code [22].

Let $\mathcal{K}$ denote a finite set of phasor kernels in $\mathbb{R}^2$. A phasor kernel $j \in \mathcal{K}$ is parametrised based on its spatial location, $\mathbf{x}_j \in \mathbb{R}^2$, its assigned unit orientation vector, $\mathbf{d}_j = \left(d_j^x, d_j^y\right)^\intercal \in \{\mathbb{R}^2 \ : \ \|\mathbf{d}_j\| = 1\}$, its signal phase shift, $\varphi_j \in [-\pi, \ \pi]$, and the globally assigned signal bandwidth, $\beta \in \mathbb{R}_{>0}$, and periodicity, $\omega \in \mathbb{R}_{>0}$. The signal $\mathcal{G}_j(\mathbf{x})$ emitted from kernel $j \in \mathcal{K}$ at the spatial location $\mathbf{x} \in \mathbb{R}^2$, is defined as

$$\mathcal{G}_j(\mathbf{x}) = \exp\left(-\beta \Delta_j(\mathbf{x})\right) \exp\left(2i\pi\omega \mathbf{d}_j \cdot (\mathbf{x} - \mathbf{x}_j) + i\varphi_j\right), \tag{7}$$

where $\Delta_j^{\mathbf{r}}(\mathbf{x})$ denotes the anisotropic distance measure given

$$\Delta_j(\mathbf{x}) = \left\| \begin{pmatrix} \frac{1}{\sqrt{2}} d_j^y & -\frac{1}{\sqrt{2}} d_j^x \\ \sqrt{2} d_j^x & \sqrt{2} d_j^y \end{pmatrix} (\mathbf{x} - \mathbf{x}_j) \right\|_2^2. \tag{8}$$

A phasor kernel therefore corresponds to a complex-valued Gabor kernel [23], as the product between an anisotropic Gaussian kernel, controlling the spatial magnitude of the emitted signal, and a complex oscillator with orientation, frequency and phase specified by the kernel parameters. From the set $\mathcal{K}$ of kernels (Fig. 3a), a phasor noise can be sampled to a finite set $\mathcal{T} \subseteq \mathbb{R}^2$ by considering the spatial average of the individual kernel signals as the complex sum

$$\mathcal{G}(\mathbf{x}) = \sum_{j \in \mathcal{K}} \mathcal{G}_j(\mathbf{x}), \ \forall \mathbf{x} \in \mathcal{T}. \tag{9}$$

The phasor noise is a complex wave-field $\mathcal{G}(\mathbf{x})$, which can be separated into its magnitude $|\mathcal{G}(\mathbf{x})|$ and phase $\mathrm{Arg}(\mathcal{G}(\mathbf{x}))$. As a trade-off between orientation conformity and periodicity adherence, branching behaviour occurs in $\mathrm{Arg}(\mathcal{G}(\mathbf{x}))$ where the magnitude of $|\mathcal{G}(\mathbf{x})|$ vanishes (Figs. 3b and 3c). To ensure connectivity of the dehomogenised design, a post-processing procedure that locally connects and reshapes the branches by an interpolation approach termed the pinch operator was introduced in [7] (Fig. 3d). This connected version of the phasor-field allows for direct projection of relative thicknesses to obtain a fluid-solid design.

Based on these outlined concepts, the phasor-based dehomogenisation approach, can for each layer of the multi-scale solution be summarised as follows:

1) Translate the homogenised solution to a sparse set of phasor kernels
2) Assign a globally fixed periodicity to all phasor kernels
3) Sample the corresponding phasor noise as a high-resolution complex wave field
4) Obtain bifurcation information from the phasor noise field magnitude
5) Obtain the perfectly oscillating real-valued wave-field from the phasor noise phase

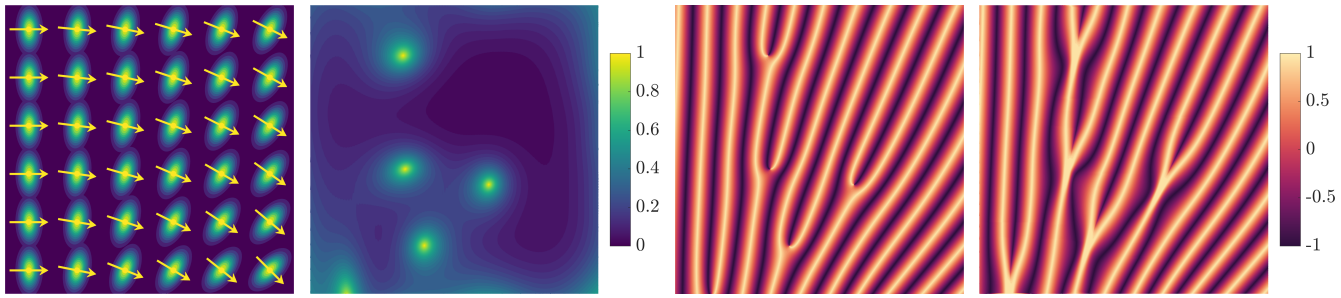

(a) Phasor kernels. (b) $\exp(-|\mathcal{G}(\mathbf{x})|)$. (c) $\sin(\text{Arg}(\mathcal{G}(\mathbf{x})))$. (d) Pinched branches.

Fig. 3: The phasor-based methodology. Given the set of phasor kernels (a), the corresponding phasor noise $\mathcal{G}(\mathbf{x})$ is sampled at a fine resolution and separated into its magnitude, highlighting singularities (b), and phase (c). Post-processing connects and pinches the bifurcations occurring from phasor field singularities (d).

6) Utilise the bifurcation information to smoothly connect disconnections in the wave-field
7) Project connected wave-field according to interpolated relative thicknesses to obtain single-scale design

The layers are then combined by a boolean union and the phasor-based boundary technique is employed to obtain a smoothed and closed body for the final design [7], [22].

D. Integrated design workflow

The integrated design workflow is summarised as follows: the process starts with initialising finite element spaces, declaring unknowns, and defining the variational formulation. Numerical homogenised material are interpolated from an offline library using a bi-linear interpolation scheme. The optimisation proceeds within a main loop. At each step, homogenisation equations are solved to obtain homogenised velocity, pressure, and temperature fields, cf. (1) and (3), followed by the evaluation of objective and constraint functions, cf. (6). Adjoint equations are solved to compute adjoint variables and sensitivities, which are then used to update the design variables using MMA. Throughout the optimisation, the phasor-based dehomogenisation can be executed on-the-fly to generate upsampled microchannel designs, cf. Section II-C, which are subsequently simulated by solving full-scale Stokes and convection-diffusion equations on a refined body-fitted mesh. The workflow is terminated after 1000 optimisation iterations.

The above-mentioned algorithm is implemented by integrating multiple tools to achieve efficiency and flexibility. The PDEs are discretised using an open-source FEA software FreeFEM [24], [25], interfaced with Python through PyFreeFEM [26], [27], allowing `.edp` scripts to serve as modular components within a larger Python project. For the optimisation process, we employ the Python implementation of the Method of Moving Asymptotes (MMA) [28], which replicates the original MATLAB implementation by Svanberg [18]. The phasor-based dehomogenisation is implemented in MATLAB [22]. A body-fitted mesh is obtained through sequential implicit mesh evolution using Mmg [29]. PETSc [30] is interfaced with FreeFEM as the distributed linear algebra backend, ensuring scalability for solving large finite element systems. All the numerical experiments are performed on a MacBook Pro mounted with a 10-core M2 Pro Apple Silicon chip.

III. Results and Discussions

In this section, we showcase a design example in Section III-A. Then, we justify the computational efficiency of the proposed framework in Section III-B by comparing it against a hypothetical brute-force full-scale optimisation scenario. Finally, in Section III-C, the limitations of the present study are discussed.

A. Numerical examples

The design setup considered in this study is illustrated in Fig. 1. In the homogenisation-based topology optimisation stage, the heat transfer is assumed to be diffusion-dominant, characterised by a low Péclet number with $\text{Pe}_\text{s} = 1/50$ for the solid phase and $\text{Pe}_\text{f} = 1$ for the fluid phase. The design field is initialised with $m_1 = 0.5$, $m_2 = 0.5$, and $\theta = 0.5$. The maximum allowable fluid phase volume fraction is set to $V_{\max} = 50\%$, while the maximum permitted pressure drop is set to 25.0. A coarse 50×50 mesh is used for the optimisation. Following this, the phasor-based dehomogenisation is conducted to reconstruct fine-scale details of the optimised microfluidic network on a 3213×3213 fine mesh, corresponding to a unit cell size of $\epsilon = 0.0125$.

Fig. 4 shows the optimised design fields after 1000 iterations (a)–(c), and the dehomogenised microchannel (d). Notably, the m_1 field (Fig. 4a) converges to a uniform value of 1.0, indicating the formation of streamline-oriented continuous long fins that extend from the low-temperature inlet to the system outlets. These fins facilitate the heat transfer through the highly conductive material. The optimised θ field (Fig. 4c) guides the fluid channels into a split-flow configuration, promoting effective flow distribution towards the two outlets.

Fig. 5 shows the velocity, pressure, and temperature fields obtained from both homogenised (top row) and full-scale (bottom row) simulations at iteration 1000. For ease of comparison, the pressure fields from the full-scale simulations are normalised by a multiplicative factor of ϵ^2 (cf. Fig. 5e). Additionally, the Péclet number in the full-scale simulation is amplified by a factor of 50 to reflect a more realistic

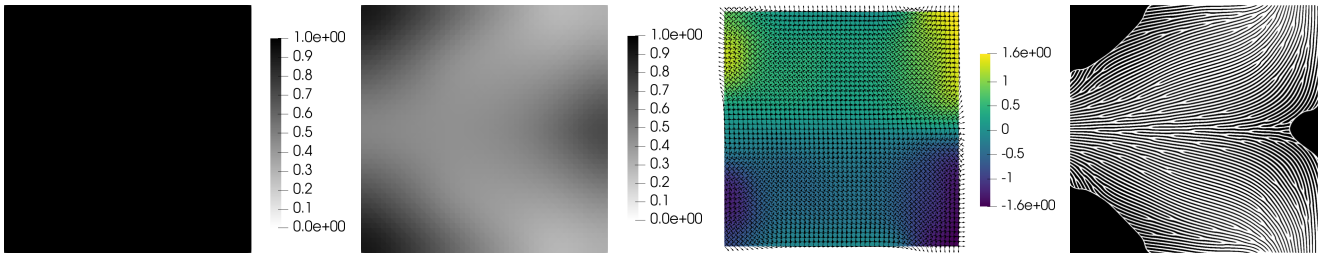

(a) m_1. (b) m_2. (c) θ. (d) Dehomogenised microchannel.

Fig. 4: Optimised design fields obtained after 1000 iterations (a)–(c). Dehomogenised microchannel design obtained by phasor-based dehomogenisation (d).

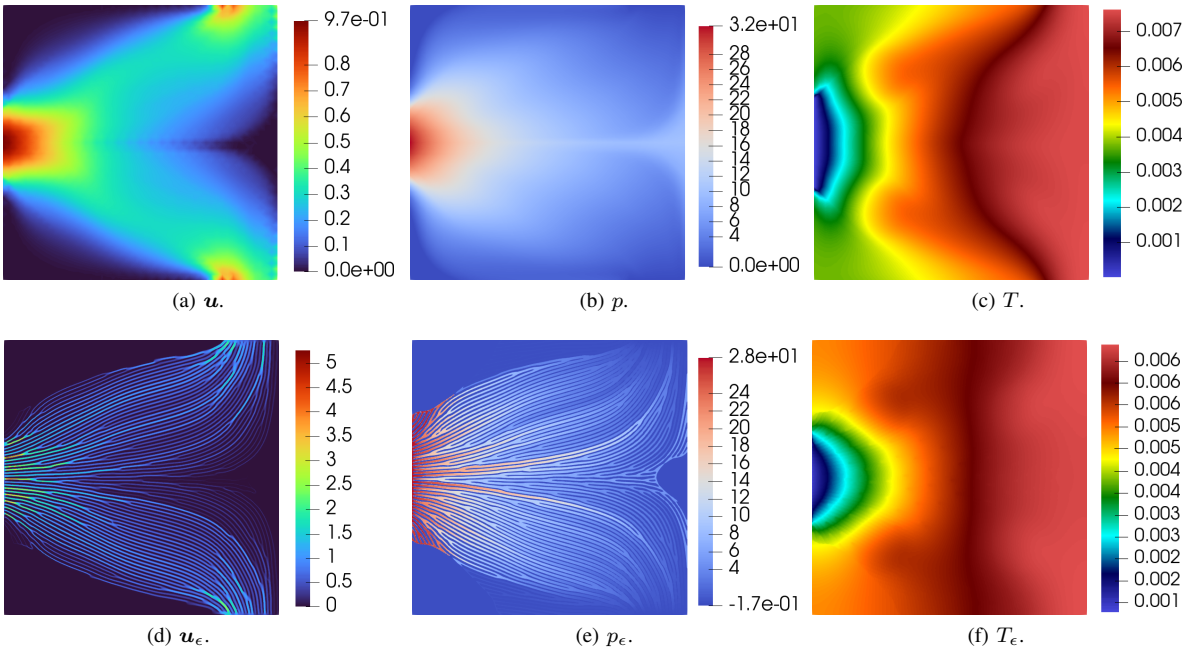

(a) $\boldsymbol{u}$. (b) p. (c) T.

(d) $\boldsymbol{u}_\epsilon$. (e) p_ϵ. (f) T_ϵ.

Fig. 5: Homogenised (top row) and dehomogenised (bottom row) solutions for velocity, pressure, and temperature fields at iteration 1000. The homogenised solutions are obtained by solving the homogenisation equations on a 50×50 grid, while the dehomogenised solutions are obtained by solving the full-scale equations on a body-fitted mesh with $1.29 \cdot 10^6$ triangluar elements in the fluid region Ω_f and $9.59 \cdot 10^5$ triangular elements in the solid region Ω_s. For comparison, the pressure fields obtained by the full-scale simulations are normalised by a multiplicative factor ϵ^2.

convection-dominant scenario. Although this adjustment introduces a theoretical simplification, due to the convection term being neglected in the homogenisation model, it supports the demonstration of the integrated workflow and underscores the potential of the proposed framework for multi-fidelity modelling.

Quantitatively, the normalised pressure drop obtained from the full-scale simulation is 26.11 (cf. Fig. 5e), corresponding to a realised pressure drop of $1.67 \cdot 10^5$. This value exceeds the maximum permitted pressure drop by 4.4%. This deviation arises from fluid channels in the dehomogenised design that connect to the external walls but not to the inlet or outlets. This issue seemes to stem from the absence of no-slip boundary conditions in the homogenised model, which struggles to capture viscous effects and fine-scale fluid-solid interface details. Several strategies could be explored for future improvements. First, redundant fluid channels with negligible flow velocity could be removed through additional post-processing. Second, adopting case-specific inlet and outlet designs, such as the circular configurations demonstrated in [31], ensures that inflow and outflow are normal to the tangential direction of the boundaries, essentially makes fluid channels connected to the inlets and outlets. However, implementing such designs necessitates the use of irregular meshes, which are yet supported by the current implementation but are theoretically feasible. Alternatively, modifications to the phasor-based dehomogenisation heuristic can also be implemented to ensure that the structural boundary connects to the inlets and outlets

directly. Additionally, modification to the design parameters m_1 and m_2, with a so-called auxiliary indicator field [32], [33], will reduce non-uniqueness to the homogenised design space, which leads to better-defined solutions and improvements in the de-homogenisation, as seen for structural problems.

The on-the-fly phasor-based dehomogenisation process is illustrated in Fig. 6, highlighting several snapshots of dehomogenised microchannel designs, velocity profiles, and temperature distributions across different iterations. The objective value reduces from $2.01 \cdot 10^{-3}$ to $1.3 \cdot 10^{-3}$ after 1000 iterations, corresponding to a 35.3% improvement. The dehomogenisation step averages $29.5\,\mathrm{s}$, outperforming the conventional projection-based methods.

B. Justification of computational efficiency

To justify the computational efficiency of the proposed design workflow, it is compared to a hypothetical brute-force fine-scale optimisation scenario. Achieving the same design resolution requires a grid size of 3213×3213, matching the resolution used for phasor-based dehomogenisation with a unit cell size of $\epsilon = 0.0125$. In the fine-scale approach, one iteration of single-scale simulation on this fine mesh, including domain decomposition, matrix assembly, right-hand-side assembly, and linear system solution, takes approximately $10\,\mathrm{min}\ 34\,\mathrm{s}$ using 10 MPI processes. As the system of equations is linear and symmetric, we can expect a similar time consumption for solving the adjoint equations. Consequently, the total optimisation time for 1000 iterations is estimated to be approximately $21\,334\,\mathrm{min}$.

In stark contrast, the homogenisation-based topology optimisation (TO) approach requires significantly fewer computational resources. Each optimisation iteration (excluding dehomogenisation and full-scale simulation) takes approximately $0.64\,\mathrm{s}$ using a single core, resulting in a total optimisation time of approximately $10\,\mathrm{min}$ for 1000 iterations. This implies a reduction in computational cost of three orders-of-magnitude compared to the brute-force fine-scale approach.

C. Limitations of the present study

The current study has several limitations to be addressed in future work that can be summarised as follows:

1) The convection effect is omitted in the unit-cell problem for convection-diffusion. Future studies will address Péclet-dominant conjugate heat transfer, encouraging hierarchical designs of microchannel networks (i.e., gray-scale in the optimised m_1 field).
2) Constructing the offline library requires solving the unit-cell problem for all parameter combinations (m_1, m_2) on a 100×100 grid within $(0, 1)^2$, excluding 0 and 1 to avoid deterioration. Partial derivatives are computed via finite differences, and linear interpolation approximates the unit square. This process is computationally intensive and could potentially be accelerated by using a surrogate model trained by deep learning.
3) Notable deviations are observed between the homogenised and full-scale velocity and pressure solutions, suggesting the need for more accurate homogenisation models and/or the adoption of multi-fidelity modelling approaches.

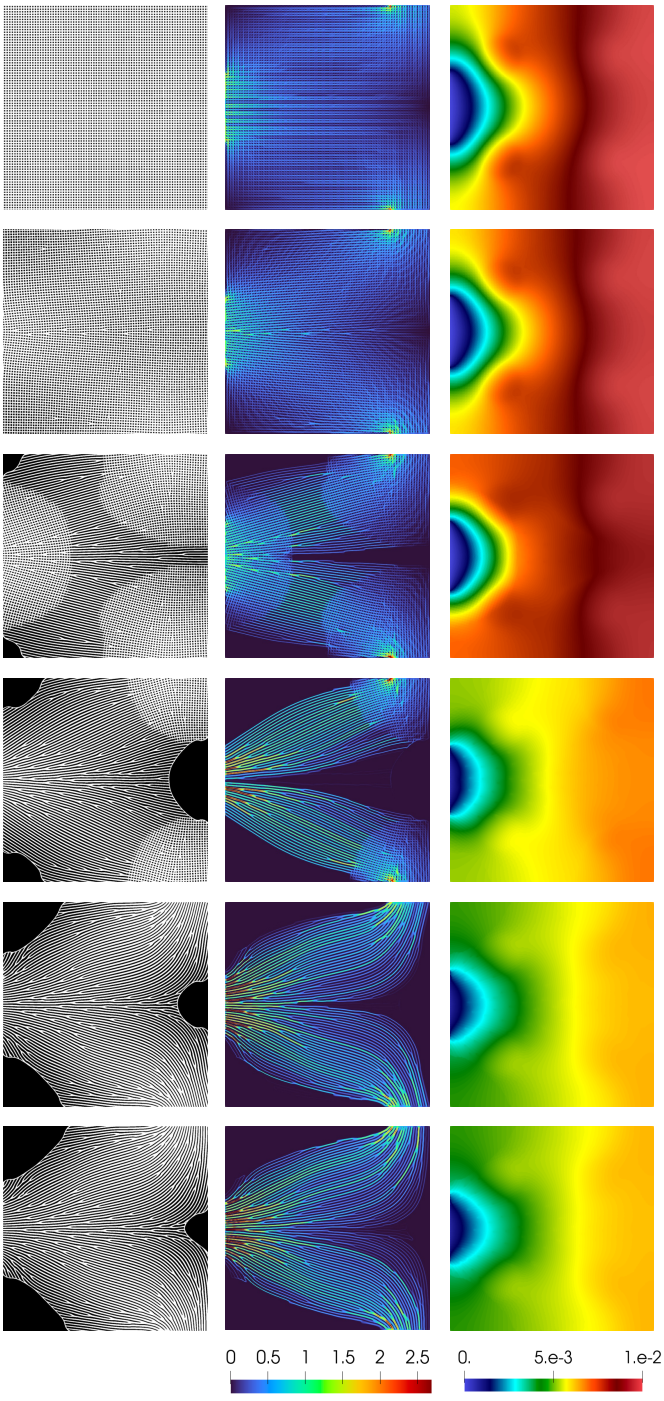

Fig. 6: On-the-fly dehomogenisation process. From left to right: snapshots of dehomogenised microchannel design (white region denotes fluid, black region denotes solid), velocity profile, and temperature distribution. From top to bottom: iterations 1, 20, 50, 100, 400, and 1000.

IV. Summary

This preliminary work proposes a multiscale design methodology for microchannel cooling networks, combining homogenisation-based topology optimisation and phasor-

based dehomogenisation, can achieve both enhanced thermal performance and computational efficiency. Specifically, the framework reduces computational costs by three orders-of-magnitude compared to fine-scale brute-force optimisation while achieving a 35.3% reduction in thermal performance compared to pin-fins. The integrated workflow effectively addresses the trade-off between pressure drop and thermal performances, enabling the design of customised cooling solutions for hotspot-aware micro-cooling systems. Future work will focus on improving the homogenisation model and exploring multi-fidelity modelling to further enhance design accuracy and applicability.

Acknowledgment

Hao Li and Joe Alexandersen gratefully acknowledge financial support from the European Union through the Marie Skłodowska-Curie Actions Postdoctoral Fellowship (grant no. 101106842).

The authors would like to express their gratitude to Dr. Pierre Jolivet from Sorbonne Université for his assistance in the construction of the FreeFEM solvers. Additionally, they extend their thanks to Professor Ole Sigmund from the Technical University of Denmark for the insightful and fruitful discussions.

References

[1] A. Boutsikakis, E. Soutter, M. S. de Troya, N. Esposito, D. Mukasheva, H. Bouras, and R. van Erp, "Glacierware: Hotspot-aware microfluidic cooling for high tdp chips using topology optimization," in *2024 30th International Workshop on Thermal Investigations of ICs and Systems (THERMINIC)*. IEEE, 2024, pp. 1–4.

[2] S. Ozguc, L. Pan, and J. A. Weibel, "Topology optimization of microchannel heat sinks using a homogenization approach," *International Journal of Heat and Mass Transfer*, vol. 169, p. 120896, 2021.

[3] S. Ozguc, P. Dionne, M. Thorsell, M. Blennius, T. Nilsson, L. Pan, and J. A. Weibel, "Experimental investigation of an additively manufactured cold plate for multi-chip module cooling generated using the homogenization approach to topology optimization," *Applied Thermal Engineering*, p. 124741, 2024.

[4] J. P. Groen and O. Sigmund, "Homogenization-based topology optimization for high-resolution manufacturable microstructures," *International Journal for Numerical Methods in Engineering*, vol. 113, no. 8, pp. 1148–1163, 2018.

[5] F. Feppon, "Multiscale topology optimization of modulated fluid microchannels based on asymptotic homogenization," *Computer Methods in Applied Mechanics and Engineering*, vol. 419, p. 116646, 2024.

[6] H. Li, P. Jolivet, and J. Alexandersen, "Multi-scale topology optimisation of microchannel cooling using a homogenisation-based method," 2024.

[7] R. V. Woldseth, J. A. Bærentzen, and O. Sigmund, "Phasor noise for dehomogenisation in 2d multiscale topology optimisation," *Computer Methods in Applied Mechanics and Engineering*, vol. 418, p. 116551, 2024.

[8] J. Wu, N. Aage, R. Westermann, and O. Sigmund, "Infill optimization for additive manufacturing—approaching bone-like porous structures," *IEEE Transactions on Visualization and Computer Graphics*, vol. 24, no. 2, pp. 1127–1140, 2017.

[9] H. Li, M. Yu, P. Jolivet, J. Alexandersen, T. Kondoh, T. Hu, K. Furuta, K. Izui, and S. Nishiwaki, "Reaction–diffusion equation driven topology optimization of high-resolution and feature-rich structures using unstructured meshes," *Advances in Engineering Software*, vol. 180, p. 103457, 2023.

[10] E. Sánchez-Palencia, "Non-homogeneous media and vibration theory," *Lecture Note in Physics, Springer-Verlag*, vol. 320, pp. 57–65, 1980.

[11] E. Sanchez-Palencia, "On the asymptotics of the fluid flow past an array of fixed obstacles," *International Journal of Engineering Science*, vol. 20, no. 12, pp. 1291–1301, 1982.

[12] T. Lévy, "Fluid flow through an array of fixed particles," *International Journal of Engineering Science*, vol. 21, no. 1, pp. 11–23, 1983.

[13] G. Allaire, "Homogenization of the navier-stokes equations in open sets perforated with tiny holes i. abstract framework, a volume distribution of holes," *Archive for Rational Mechanics and Analysis*, vol. 113, pp. 209–259, 1991.

[14] ——, "Homogenization of the navier-stokes equations in open sets perforated with tiny holes ii: Non-critical sizes of the holes for a volume distribution and a surface distribution of holes," *Archive for rational mechanics and analysis*, vol. 113, pp. 261–298, 1991.

[15] F. Feppon, "Asymptotic expansions of Stokes flows in finite periodic channels," Feb. 2024, working paper or preprint. [Online]. Available: https://hal.science/hal-04443652

[16] E. Sanchez-Palencia, "Fluid flow in porous media," *Non-homogeneous media and vibration theory*, pp. 129–157, 1980.

[17] E. Andreassen and C. S. Andreasen, "How to determine composite material properties using numerical homogenization," *Computational Materials Science*, vol. 83, pp. 488–495, 2014.

[18] K. Svanberg, "The method of moving asymptotes—a new method for structural optimization," *International journal for numerical methods in engineering*, vol. 24, no. 2, pp. 359–373, 1987.

[19] T. Tricard, S. Efremov, C. Zanni, F. Neyret, J. Martínez, and S. Lefebvre, "Procedural phasor noise," *ACM Trans. Graph.*, vol. 38, no. 4, jul 2019. [Online]. Available: https://doi.org/10.1145/3306346.3322990

[20] T. Tricard, V. Tavernier, C. Zanni, J. Martínez, P. A. Hugron, F. Neyret, and S. Lefebvre, "Freely orientable microstructures for designing deformable 3D prints," Tech. Rep. 6, 2020.

[21] A. Lagae, S. Lefebvre, R. Cook, T. DeRose, G. Drettakis, D. Ebert, J. Lewis, K. Perlin, and M. Zwicker, "A Survey of Procedural Noise Functions," *Computer Graphics Forum*, vol. 29, no. 8, pp. 2579–2600, 12 2010.

[22] R. V. Woldseth, O. Sigmund, and P. D. L. Jensen, "An 808 line phasor-based dehomogenisation matlab code for multi-scale topology optimisation," *Structural and Multidisciplinary Optimization*, vol. 67, no. 12, p. 205, 2024.

[23] A. Lagae, S. Lefebvre, G. Drettakis, and P. Dutré, "Procedural Noise Using Sparse Gabor Convolution," in *ACM SIGGRAPH 2009 Papers*, ser. SIGGRAPH '09. New York, NY, USA: Association for Computing Machinery, 2009. [Online]. Available: https://doi.org/10.1145/1576246.1531360

[24] F. Hecht, "New development in FreeFem++," *Journal of Numerical Mathematics*, vol. 20, no. 3-4, pp. 251–266, 2012.

[25] P. Jolivet, V. Dolean, F. Hecht, F. Nataf, C. Prud'homme, and N. Spillane, "High-Performance Domain Decomposition Methods on Massively Parallel Architectures with FreeFem++," *Journal of Numerical Mathematics*, vol. 20, no. 4, pp. 287–302, 2012.

[26] F. Feppon, "Shape and topology optimization of multiphysics systems," Ph.D. dissertation, Paris Saclay, 2019.

[27] ——, "Density-based topology optimization with the null space optimizer: a tutorial and a comparison," *Structural and Multidisciplinary Optimization*, vol. 67, no. 1, p. 4, 2024.

[28] A. Deetman, "Gcmma-mma-python: Python implementation of the method of moving asymptotes," oct 2024. [Online]. Available: https://zenodo.org/record/13337495

[29] G. Allaire, C. Dapogny, and P. Frey, "A mesh evolution algorithm based on the level set method for geometry and topology optimization," *Structural and Multidisciplinary Optimization*, vol. 48, no. 4, pp. 711–715, 2013.

[30] S. Balay, S. Abhyankar, M. F. Adams, S. Benson, J. Brown, P. Brune, K. Buschelman, E. Constantinescu, L. Dalcin, A. Dener, V. Eijkhout, J. Faibussowitsch, W. D. Gropp, V. Hapla, T. Isaac, P. Jolivet, D. Karpeev, D. Kaushik, M. G. Knepley, F. Kong, S. Kruger, D. A. May, L. C. McInnes, R. T. Mills, L. Mitchell, T. Munson, J. E. Roman, K. Rupp, P. Sanan, J. Sarich, B. F. Smith, S. Zampini, H. Zhang, H. Zhang, and J. Zhang, "PETSc/TAO users manual," Argonne National Laboratory, Tech. Rep. ANL-21/39 - Revision 3.19, 2023.

[31] Y. Zhou, D. J. Lohan, F. Zhou, T. Nomura, and E. M. Dede, "Inverse design of microreactor flow fields through anisotropic porous media optimization and dehomogenization," *Chemical Engineering Journal*, vol. 435, p. 134587, 2022.

[32] R. Giele, J. Groen, N. Aage, C. S. Andreasen, and O. Sigmund, "On approaches for avoiding low-stiffness regions in variable thickness sheet and homogenization-based topology optimization," *Structural and Multidisciplinary Optimization*, vol. 64, p. 39–52, 2021.

[33] P. D. L. Jensen, O. Sigmund, and J. P. Groen, "De-homogenization of optimal 2d topologies for multiple loading cases," *Computer Methods in Applied Mechanics and Engineering*, vol. 399, p. 115426, 2022.